Chemical Science

ROYAL SOCIETY OF CHEMISTRY

EDGE ARTICLE

View Article Online
View Journal | View Issue

Cite this: *Chem. Sci.*, 2024, **15**, 4019

All publication charges for this article have been paid for by the Royal Society of Chemistry

Molecular engineering of AIE-active boron clustoluminogens for enhanced boron neutron capture therapy†

Wenli Ma,‡[a] Yanyang Wang,‡[b] Yilin Xue,[c] Mengmeng Wang,[a] Changsheng Lu,[a] Wanhua Guo,[d] Yuan-Hao Liu,[efg] Diyun Shu,[efg] Guoqiang Shao,[c] Qinfeng Xu,*[h] Deshuang Tu*[a] and Hong Yan*[a]

The development of boron delivery agents bearing an imaging capability is crucial for boron neutron capture therapy (BNCT), yet it has been rarely explored. Here we present a new type of boron delivery agent that integrates aggregation-induced emission (AIE)-active imaging and a carborane cluster for the first time. In doing so, the new boron delivery agents have been rationally designed by incorporating a high boron content unit of a carborane cluster, an erlotinib targeting unit towards lung cancer cells, and a donor–acceptor type AIE unit bearing naphthalimide. The new boron delivery agents demonstrate both excellent AIE properties for imaging purposes and highly selective accumulation in tumors. For example, at a boron delivery agent dose of 15 mg kg^{-1}, the boron amount reaches over 20 μg g^{-1}, and both tumor/blood (T/B) and tumor/normal cell (T/N) ratios reach 20–30 times higher than those required by BNCT. The neutron irradiation experiments demonstrate highly efficient tumor growth suppression without any observable physical tissue damage and abnormal behavior *in vivo*. This study not only expands the application scopes of both AIE-active molecules and boron clusters, but also provides a new molecular engineering strategy for a deep-penetrating cancer therapeutic protocol based on BNCT.

Received 21st November 2023
Accepted 1st February 2024

DOI: 10.1039/d3sc06222h

rsc.li/chemical-science

Introduction

The research and development of boron-containing functional molecules have attracted extensive attention and represent a cutting-edge frontier in chemistry owing to the unique electronic structure and properties of the boron atom.[1] It is noteworthy that a ^{10}B atom possesses a high neutron-capture cross-section (3835 barns), which renders ^{10}B-based molecules highly desirable as neutron capture agents for boron neutron capture therapy (BNCT). The fundamental principle of BNCT is based on the nuclear reaction that upon irradiation by thermal neutrons, a ^{10}B atom releases an alpha particle ($^{4}He^{2+}$) and recoil lithium nucleus ($^{7}Li^{3+}$), which enables the killing of a cancer cell in a mode of inside one single cell (5–9 μm). Thus BNCT could minimize damage to healthy tissues which makes it an advanced binary and cell-level radiotherapy.[2,3] However, the clinical applications of BNCT were severely hampered because known boron delivery agents such as BPA (boronophenylalanine) and BSH (sodium mercaptoundecahydro-*closo*-dodecaborate)[2f,g] (Fig. 1a) have issues such as low boron content (BPA), low *in vivo* stability and solubility, poor biocompatibility, and lack of targeting and imaging. Currently, the key issue for BNCT is the development of a new generation of boron delivery agents that can fulfil the requirements of BNCT.

BNCT requires delivery agents containing a substantial boron content.[2] Notably, icosahedral carboranes (*i.e.*, $C_2B_{10}H_{12}$) are a type of classical boron-enriched clusters bearing diverse properties[4] such as low toxicity, biocompatibility, unique electronic properties, three-dimensional aromaticity, large size, tunable hydrophobicity and hydrophilicity, and high chemical and thermal stabilities. Thus carboranes have been extensively used for biological activity studies,[5] luminescent materials,[6]

[a]*State Key Laboratory of Coordination Chemistry, Jiangsu Key Laboratory of Advanced Organic Materials, School of Chemistry and Chemical Engineering, Nanjing University, Nanjing 210023, China. E-mail: hyan1965@nju.edu.cn*
[b]*Department of Nuclear Medicine, Nanjing Drum Tower Hospital, Affiliated Hospital of Medical School, Nanjing University, Nanjing 210008, China*
[c]*Department of Nuclear Medicine, Nanjing First Hospital, Nanjing Medical University, Nanjing 210033, China*
[d]*Department of Nuclear Medicine, Nanjing Tongren Hospital, the Affiliated Hospital of Southeast University Medical School, Nanjing 210033, China*
[e]*Neuboron Therapy System Ltd., Xiamen 361028, China*
[f]*Nanjing University of Aeronautics and Astronautics, Nanjing 210016, China*
[g]*Neuboron Medtech Ltd., Nanjing 211112, China*
[h]*Department of Nuclear Medicine, Jiangsu Province Hospital of Chinese Medicine, Affiliated Hospital of Nanjing University of Chinese Medicine, Nanjing 210029, China*

† Electronic supplementary information (ESI) available. See DOI: https://doi.org/10.1039/d3sc06222h

‡ These authors contributed equally to this work.

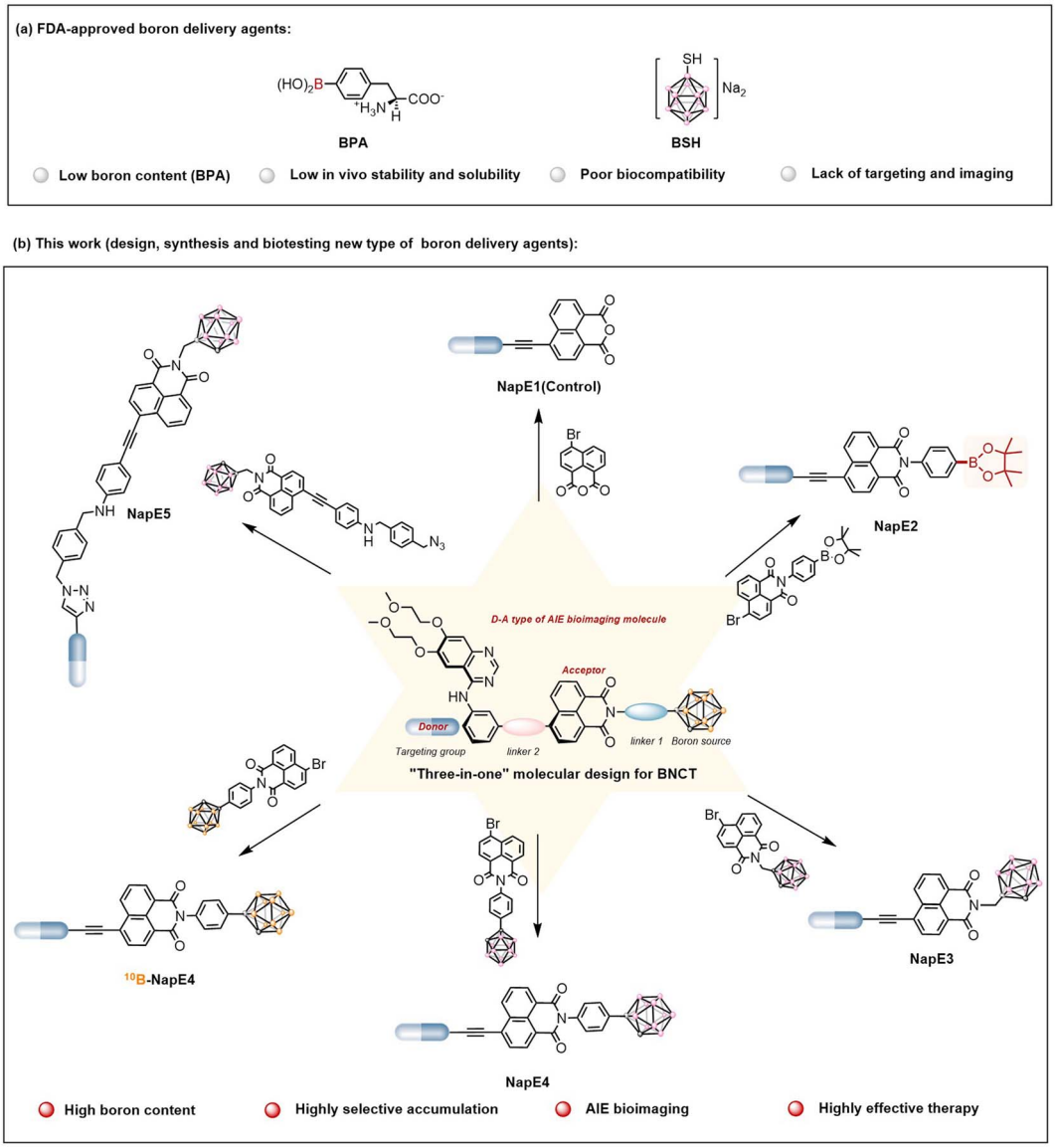

Fig. 1 (a) Two FDA-approved boron delivery agents for BNCT. (b) New boron delivery agents for BNCT based on the "three-in-one" molecular design strategy (this work).

bioimaging[7] and others.[8] In particular, carboranes have also been utilized to design delivery agents for BNCT investigations, which have demonstrated different effectiveness *in vitro* and *in vivo*.[9] Despite these important advances, the development of carborane-based delivery agents is sporadic and still faces challenges such as low biocompatibility, inadequate tumor accumulation, low tumor/blood (T/B) and tumor/normal cell (T/N) ratios, and lack of imaging. Undoubtedly, the development of multifunctional boron-enriched delivery agents with high biocompatibility, targeting, imaging, and therapeutic efficacy will hold great potential for high-performance applications in BNCT for both diagnosis and treatment.

Among various imaging techniques, fluorescence imaging is a useful tool for non-invasive cancer diagnosis. However, traditional luminogens used for biological imaging usually suffer from the aggregation-caused quenching effect,[10a] which restricts the working concentration in biological systems. In particular, BNCT requires extremely high boron content (>10^9 ^{10}B atoms/per cancer cell) accumulated inside tumor cells. As such, aggregation-induced emission luminogens (AIEgens) are appropriate for bioimaging in the design of multifunctional delivery agents as they can exhibit bright emission in an aggregate state, excellent photobleaching resistance, and a high signal-to-noise ratio.[10] Until now, by means of the rational design of AIEgens, biomedical applications related to AIE-active imaging have been developed including real-time tracing,[11] fluorescence sensing,[12] tumor imaging,[13] photodynamic therapy (PDT),[14] photothermal therapy (PTT),[15] surgical navigation,[16] and immunotherapy.[17] Nevertheless, to the best of our knowledge, AIEgens have not yet been reported in BNCT investigations. Based on the above considerations, AIEgens should be ideal tracking reagents for BNCT for visualization purposes.

To address the aforementioned issues in boron delivery agents for BNCT applications, in this study, a new molecular platform that integrates AIE-active imaging with a boron-enriched cluster to construct a new type of boron delivery agent was developed for the first time. As a proof of concept, boron delivery agents based on a "three-in-one" strategy were designed by incorporating a high boron content unit of carborane, an Eriotinib-based lung cancer targeting unit, and a D–A (donor–acceptor) type AIE imaging unit using naphthalimide as a strong acceptor (Fig. 1b). Such a molecular system exhibited the expected AIE properties with red emissions, negligible toxicity and excellent biocompatibility. More importantly, highly selective ^{10}B accumulation (>20 μg g^{-1}) inside lung cancer cells was achieved even when a low dose (15 mg kg^{-1}) of the boron delivery agent **^{10}B-NapE4** was applied (for comparison, the dose of BPA for the treatment of melanoma used was 600 mg kg^{-1} to give a ^{10}B accumulation of 36 ± 4 μg g^{-1} (ref. 2b)). In particular, the T/B and T/N ratios reached up to 30 : 1, far beyond 3 : 1 as required by BNCT. Under AIE imaging, satisfactory outcomes have been obtained as evidenced by efficient tumor growth inhibition on A549 tumor-bearing mice (a model for lung cancer) with no physical tissue damage and abnormal behavior during a 10-day observation after neutron irradiation. This work presents multiple functionalized boron delivery agents for BNCT investigations and expands the type of tumors applicable to BNCT. The findings may demonstrate that BNCT is not only suitable for superficial cancers such as melanoma, and head and neck cancers, but also has great potential in deep-penetrating cancer treatment.

Results and discussion

"Three-in-one" molecular design of boron delivery agents

The two clinically used boron delivery agents as shown in Fig. 1a[2a] have either inadequate boron content or inadequate targeting function, and both also lack imaging capability. In this study, to address these issues, we proposed a "three-in-one" strategy for molecular design which includes a boron source as a pharmacophore, a targeting functional group to deliver boron delivery agents into the targeted tumors, and an imaging functional unit to track the pathways of a boron delivery agent (Fig. 1b). Despite valuable progress in other boron-containing carriers,[18] here a carborane cluster was chosen as a boron source owing to its advantages such as high boron content (*i.e.*, one carborane cluster contains ten boron atoms), high stability, and low toxicity.[5] On the other hand, previous BNCT treatments focused on superficial cancers such as melanoma, head and neck cancers, and brain glioma. In this study, we explored the possibility of treating deep-penetrating cancers, for instance, lung tumors. In doing so, the widely used non-small cell lung cancer-targeting drug, Eriotinib, was selected as a targeting moiety to deliver boron delivery agents to obtain sufficient boron accumulation in tumors. It is noted that Eriotinib was approved as a small-molecule-targeted epidermal growth factor receptor (EGFR) inhibitor by the Food and Drug Administration (FDA) in 2004,[19] and exhibits a specific affinity to tumor cells by targeting the adenosine triphosphate binding domain of tyrosine kinase in EGFR-overexpressing tumors.[20] Moreover, to achieve real-time tracking of boron delivery agents, an imaging unit needs to be incorporated. As BNCT requires a very high boron amount inside cancer cells, the boron delivery agents are optimally designed as AIEgens to ensure the effectiveness of imaging. Based on the AIE working mechanism,[10] luminogens with intramolecular charge transfer are capable of exhibiting AIE properties. As such, we exploited the chromophore of naphthalimide in molecular design as a strong electron acceptor since naphthalimide has been commonly used for biological imaging.[21] Notably, here the carborane moiety is also a three-dimensional steric group that can enhance AIE emission, and for the first time Eriotinib acts as an electron donor to be used in the construction of luminogens. Thus the D–A type of AIE-active luminescent boron delivery agents have been drafted, denoted as **NapE3-5**, as depicted in Fig. 1b. Such an integration of the molecular moieties of naphthalimide, carborane and Eriotinib may lead to AIE properties for the expected boron delivery agents.

Preparation and characterization of the NapE compounds

To synthesize the above-designed boron delivery agents, we initially used the $B_{10}H_{12}(CH_3CN)_2$ precursor to react with naphthalimide-substituted alkynes to obtain carborane-conjugated naphthalimide intermediates in moderate yields. The targeted products **NapE3-5** were generated by the use of either the classic Sonogashira reaction or copper(I)-catalyzed azide-alkyne cycloaddition in high yields. In addition, the control compounds **NapE1** without a boron atom and **NapE2** containing one boron atom were also synthesized for comparison (Fig. 1b, 2, S1 and Schemes S1–S5†). All of these compounds were thoroughly characterized by using Fourier transform infrared (FT-IR) spectra (Fig. S2†), NMR spectra (Fig. S21–S33†), and high-resolution mass spectrum (HRMS), as shown in the ESI.†

Photophysical properties of the NapE compounds

With the carborane-based compounds in hand, the photophysical properties were investigated to examine the above molecular design (Fig. 3a, S3, Tables S1 and S2†). In solution, the absorption bands of **NapE** compounds were observed within the range of 300–500 nm. The long-wavelength absorption band is beneficial for the molecular imaging study. **NapE1-4** exhibits a comparable absorption spectral profile while **NapE5** displays a more red-shifted absorption band which could be attributed to the strong electron-donating ability of the *N*-alkyl phenyl group. All the absorption bands for **NapE1-5** arise from charge transfer, as supported by the separate electronic distributions of HOMOs (highest occupied molecular orbitals) and LUMOs (lowest unoccupied molecular orbitals) in the ground state (Fig. 3b and S4†). The photoluminescence (PL) spectra of **NapE1-5** show broad emission bands with large Stokes shifts beyond 100 nm (Fig. S3b and Table S1†). Besides, the emission peaks range from 523 to 664 nm and are red-shifted in comparison to those of the individual Eriotinib and naphthalimide.[20f,21d] The emissions should originate from the charge

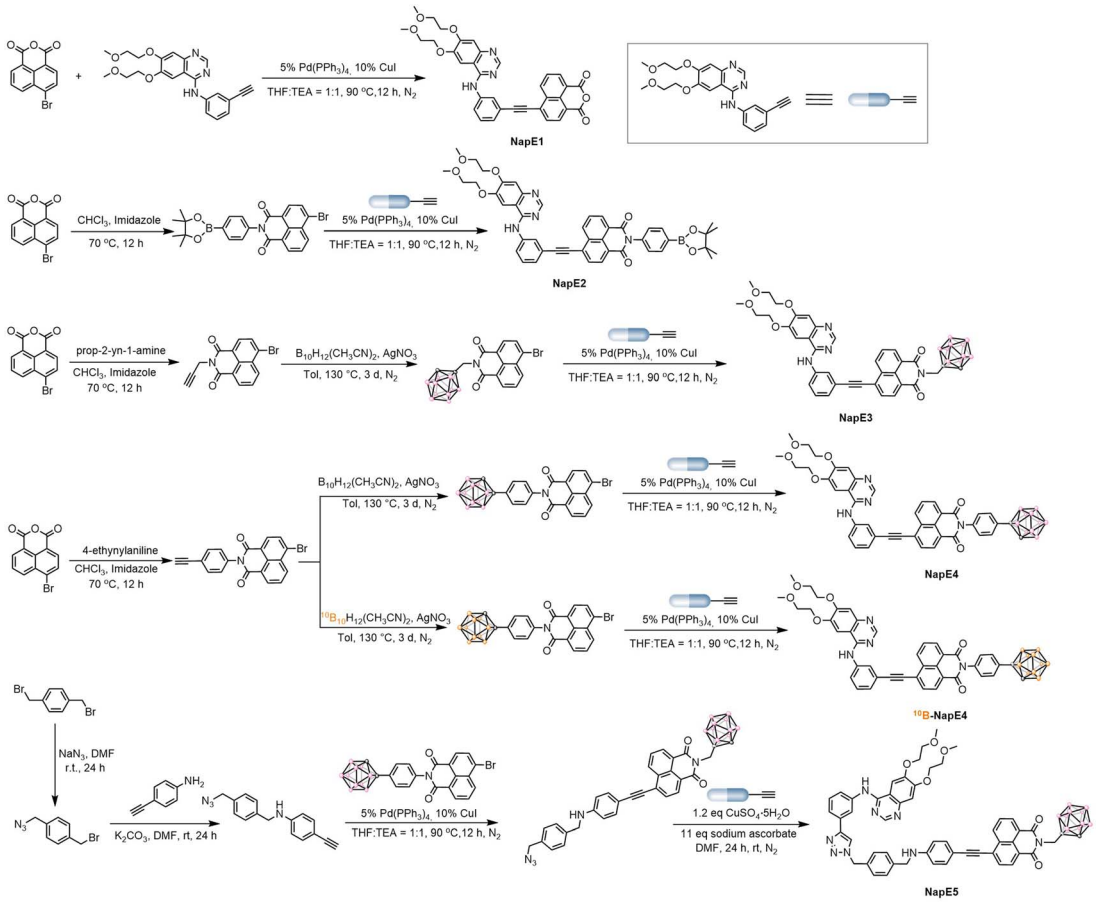

Fig. 2 Synthesis of five carborane-based boron delivery agents.

transfer state.[6h] In particular, **NapE5** shows a deep red emission with a CIE (Commission Internationale de l'Eclairage) coordinate of (0.68, 0.32) (Fig. S3c†) due to the strong electron-donating ability of *N*-alkyl phenyl. To confirm CT emission, PL spectra in different solvents were investigated for **NapE1-5** (Fig. S5 and Table S3†). They all show solvatochromic luminescence where upon increasing the polarity of the solvent, a more bathochromic emission appears. This indicates that the excited luminophore is in balance with the solvent, leading to a strong dependence on solvent polarity.[22] Further theoretical calculations[23] also reveal that the hole localizes on the Eriotinib unit, whereas the electron resides on phenyl and partial naphthalimide (Fig. S6†). All the observations demonstrate a charge transfer emission feature, consistent with the D–A type structural design for luminescence. We further evaluated the AIE properties of **NapE4-5** by using DMSO and water-mixed solvents (Fig. 3c–e and S7†). In DMSO solution, weak emissions were observed for the two compounds. These should be attributed to intramolecular charge transfer emission in a polar solvent, which leads to strong non-radiative decay in the excited state in solution. The finding is in accordance with classical ICT-based molecular systems.[11] Upon increasing the water fraction (f_w), the PL intensity was increased, which reached the maximum at $f_w = 99\%$. To validate the enhancement of PL emission triggered by molecular aggregation, both dynamic light scattering (DLS) and transmission electron microscopy (TEM) were used to verify the formation of nanoparticles. As illustrated in Fig. S8,† at $f_w =$ 99% an average diameter of 100–160 nm was observed for **NapE4-5**. The zeta-potential values **of NapE4** and **NapE5** in aqueous solution (Fig. S8c†) were measured to be −27 and −54 mV, respectively. Next, we measured the absolute quantum yields of **NapE4-5** in DMSO to be 1.0% and 2.0%, respectively, and in the mixed DMSO/water at f_w = 99% to be 5.6% and 11.4%, respectively. The above results demonstrate the AIE properties for the designed molecular system. The AIE mechanism of **NapE4-5** is attributed to the restriction of molecular motions.[10] In solution, strong non-radiative decay occurs in the excited state due to molecular motions, particularly the rotation at the ethynyl linker, which results in weak emission. However, when aggregated, the easy molecular motions in solution are suppressed. On the other hand, a large-size carborane cluster can also disrupt non-specific intermolecular interactions that usually cause concentration quenching. Consequently, enhanced emission can be observed in aggregates. Besides, Eriotinib is also approved as a good electron donor for AIEgen design. Thereby this study provides the first example of an Eriotinib-based D–A molecular system and demonstrates multiple applications of Eriotinib.

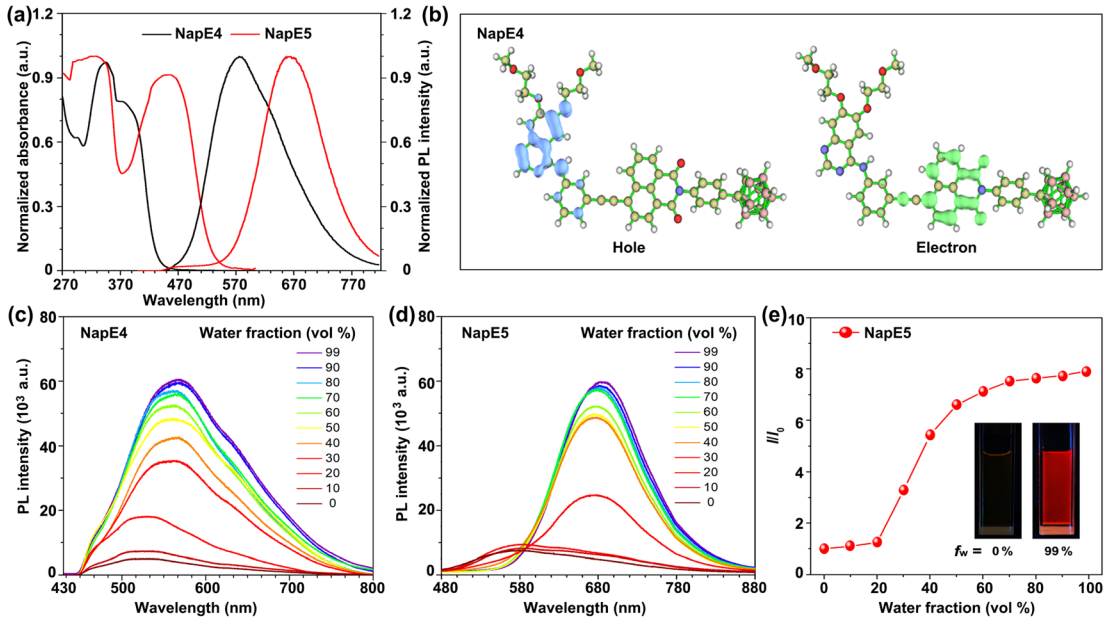

Fig. 3 (a) Normalized UV-vis absorption spectra (left side) and PL spectra (right side) at room temperature in the mixed solvents for **NapE4-5** (the volume ratio between PBS buffer solution and DMSO = 95 : 5, 10 μM, λ_{ex} = 365 nm). (b) HOMO and LUMO distributions of **NapE4** in the ground state. PL spectra of **NapE4** (c) and **NapE5** (d) in mixed DMSO/water with different water fractions (f_w). (e) The plot of the relative emission intensity (I/I_0) *versus* water fraction. I_0 and I are the peak values of PL intensities of **NapE5** in DMSO and DMSO/water mixtures, respectively. Inset: luminescence photograph.

Cytotoxicity, cellular uptake and localization of NapE compounds

As BNCT requires low cytotoxicity for boron delivery agents, the cytotoxicity of **NapE1-5** on the A549 lung cancer cells was examined by CCK8 assay. Except for **NapE2**, they all exhibited negligible cytotoxic effect on A549 cells at concentrations lower than 60 μM at 24 h, 48 h and even 72 h, respectively (Fig. S9†). The cytotoxicity of carborane-based **NapE3-5** is less than that of the one-boron-atom-containing compound **NapE2**. Specifically, no cytotoxicity was observed even at a concentration of 100 μM for **NapE5**. These results reveal that the carborane moiety not only provides high boron content, but also reduces the cytotoxicity of **NapE** compounds. Next, the stability of **NapE1-5** was examined in a physiological environment, and showed no observable change in the UV-vis absorption intensity after 72 h of incubation in a PBS buffer solution (Fig. S10†). Thus, **NapE1-5** was considered for further biological imaging applications. Firstly, the initial inspection of the uptake of **NapE1-5** in A549 cells was performed by confocal microscopy, which showed that the fluorescence intensity of **NapE4-5** was considerably higher than that of **NapE2-3** at 48 h (Fig. S11†). Next **NapE4-5** was selected to monitor the cellular uptake of A549 cells at a concentration of 60 μM for different time periods. The microscopy images showed that **NapE4-5** could be transported to the cytoplasm of lung cancer cells and reached the maximum around 48 h culture (Fig. 4a and S12†). Besides, a good overlap of fluorescence imaging between **NapE4-5** and EGFR was observed (Fig. 4a and S12†). Notably, owing to the advantage of AIE properties, both boron delivery agents exhibited bright imaging in cancer cells even at a concentration of 60 μM (Fig. S12†). Secondly, we further evaluated the cellular uptake of **NapE4-5** in A549 cells by inductively coupled plasma mass spectrometry (ICP-MS). The boron content reached 68.85 ± 9.58 ng/10^6 cells at 24 h, 217.90 ± 5.08 ng/10^6 cells at 48 h and 132.54 ± 4.35 ng/10^6 cells at 72 h for **NapE4** (Fig. 4b and Table S4†). For **NapE5**, the boron content reached 29.06 ± 4.03 ng/10^6 cells at 24 h, 46.28 ± 1.73 ng/10^6 cells at 48 h, and 41.83 ± 3.44 ng/10^6 cells at 72 h (Fig. 4b and Table S4†). It is clear that **NapE4** enters A549 cells more quickly and efficiently, which might be attributed to its relatively lower molecular weight (806.4107 g mol^{-1}) in comparison to **NapE5** (1006.5148 g mol^{-1}).

To demonstrate the generality of the molecular design, H2228 cancer cells (low-sensitive lung cancer cells) were also selected and incubated with **NapE4-5** to test the intracellular boron content. To our delight, more fast and higher uptake (*i.e.* **NapE4**: 293.36 ± 4.35 ng/10^6 cells at 72 h and **NapE5**: 78.41 ± 4.03 ng/10^6 cells at 24 h) was obtained (Fig. S12, 13 and Table S4†). The ICP-MS analytical results are well consistent with the AIE fluorescence indication, demonstrating the significance of bioimaging in this research. Moreover, BEAS-2B cells, human bronchial epithelial cells, were also incubated with **NapE4-5** to test cytotoxicity and intracellular boron content (Fig. S9g–h, S13c and Table S4†). The results showed that the two compounds have no cytotoxicity on normal cells and the intracellular boron contents in normal cells are much lower than those in lung cancer cells. The aforementioned findings suggest that the incorporation of an Eriotinib unit into **NapE4-5** has led to high uptake in both highly sensitive and low sensitive lung cancer cells. These results have established a basis for a subsequent *in vivo* imaging study.

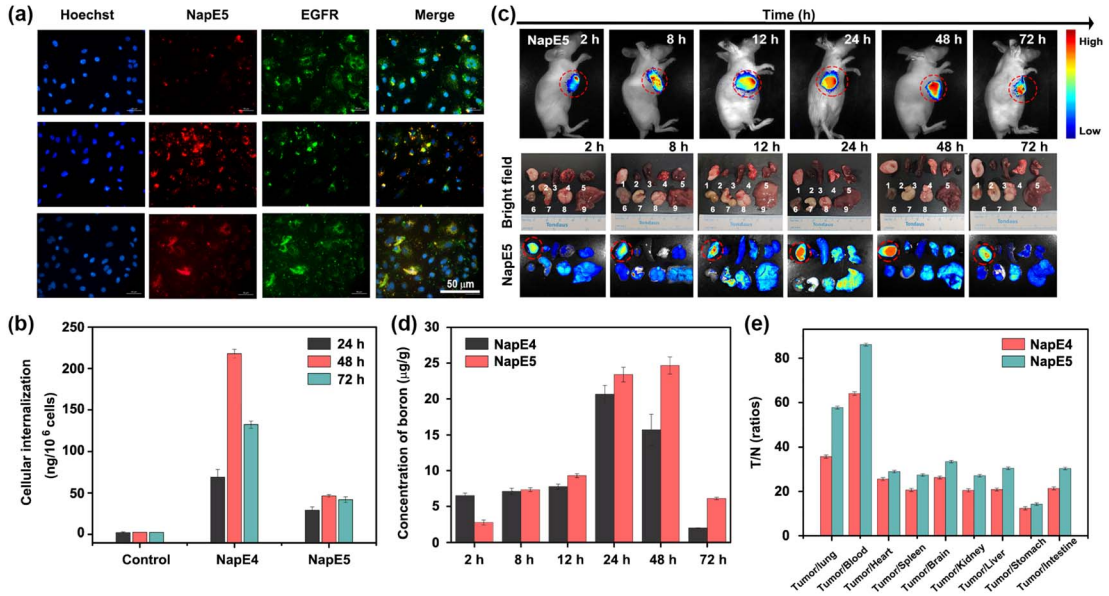

Fig. 4 (a) Confocal microscopy images of A549 cells incubated with **NapE5** (60 μM), Hoechst and EGFR (24 h, 48 h, 72 h; **NapE5**, $\lambda_{ex} = 559$ nm and $\lambda_{em} = 600–720$ nm; EGFR, $\lambda_{ex} = 488$ nm and $\lambda_{em} = 500–600$ nm; Hoechst: $\lambda_{ex} = 405$ nm and $\lambda_{em} = 400–500$ nm), scale bar = 50 μm. (b) The boron content of A549 cells incubated with **NapE4-5** (60 μM). (c) Fluorescence images of A549 tumor-bearing mice and organs at different times after intravenous injection of 15 mg kg^{-1} of **NapE5**. 1: tumor; 2: heart; 3: spleen; 4: lung; 5: kidney; 6: intestine; 7: stomach; 8: brain; 9: liver (**NapE5**: $\lambda_{ex} = 455$ nm and $\lambda_{em} = 580–750$ nm). (d) The boron content of **NapE4-5** internalized in the A549 tumor-bearing mice at different times. (e) The T/N ratio of the boron content of different organs from A549 tumor-bearing mice at 24 h for **NapE4-5**.

In vivo imaging and biological distribution of NapE4-5

The boron content in tumors is a crucial factor for the therapeutic efficacy of BNCT. To track the dynamic biological distribution of boron delivery agents, fluorescence navigation continued to be employed. As shown in Fig. 4c and S14,† **NapE4-5** reached the maximum concentrations in the lung tumors in the period of 24–48 h of administration at a dose of 15 mg kg^{-1}. Such a retention time period is sufficient for further experiments. To our delight, the images of other organs in mice showed that the fluorescence intensities are rather weak, demonstrating that targeting delivery has been achieved for the two compounds (Fig. 4c and S14†). Moreover, bioimaging could show a time-dependent distribution of compounds in mice (Fig. S14 and S15†), and therefore, the delivery of two boron delivery agents could be *in vivo* monitored.

To quantify the uptake of the boron delivery agents *in vivo*, the boron content in different organs at different times was measured by ICP-MS (Fig. 4d, e and Tables S5–S8†). For **NapE4**, the boron accumulation in tumors was measured to be 20.66 ± 1.23 μg g^{-1} (tumors) after 24 h of injection. In sharp contrast, the uptake in other organs such as the lung, brain, kidney, liver, spleen, stomach, small intestine, heart and blood was quite lower (<1.67 μg g^{-1}, Table S5 and Fig. S16a†), and a higher T/N of 35.70 ± 0.73 and T/B of 64.03 ± 0.78 were obtained (Fig. 4e, S16c and Table S6†). **NapE5** demonstrated better results for boron accumulation: 23.41 ± 1.02 μg g; T/N = 57.70 ± 0.63; T/B = 86.17 ± 0.65 at 24 h (Fig. 4e, S16b, d, Tables S7 and S8†). Similarly, **NapE5** showed very low uptake in other organs (<1.65 μg g^{-1}, Table S7†). These data exceed the values required by BNCT (*i.e.* boron accumulation of 20 μg g^{-1}, T/N = 3 and T/B = 3), demonstrating the excellent tumor selectivity of the carborane-based boron delivery agents. Note that **NapE5** showed longer retention in tumor cells than **NapE4** (Fig. 4d), which might be attributed to its molecular size. Again, a strong correlation between the boron content measured by ICP-MS and the fluorescence imaging outcomes *in vivo* was observed. These results have proven our molecular design on both targeted delivery and imaging tracking, which lay the foundation for high efficacy and biosafety upon neutron irradiation. Further hematoxylin and eosin (H&E) staining analyses of the main organs, which were harvested on the 7th day, showed no evident pathological damage or change. This indicates that the compounds have good biocompatibility *in vivo* (Fig. S17†) and are suitable for further neutron irradiation experiments.

Neutron irradiation of cells

After consideration of the synthesis and biological activity, **NapE4** was chosen for further neutron irradiation experiments. As such, **NapE4** was replaced by ^{10}B-enriched **^{10}B-NapE4** (Fig. 5a), which was synthesized as shown in Fig. 1b, 2 and Scheme S5.† The photophysical properties of **^{10}B-NapE4** and its cellular uptake at 48 h were measured again (Fig. S3d, e and Table S9†), and are similar to those of **NapE4**. Next, A549 cells were treated with different concentrations of **^{10}B-NapE4** for 48 h, and then exposed to neutron irradiation with different doses (low dose: 17 min and high dose: 26 min). After this, the irradiated cells were cultured to examine cell viability. As a result, the cell proliferation was considerably inhibited with an increased concentration of **^{10}B-NapE4** (Fig. 5b, S18a and b†). After 72 h the cell proliferation was reduced by 67.7% (for

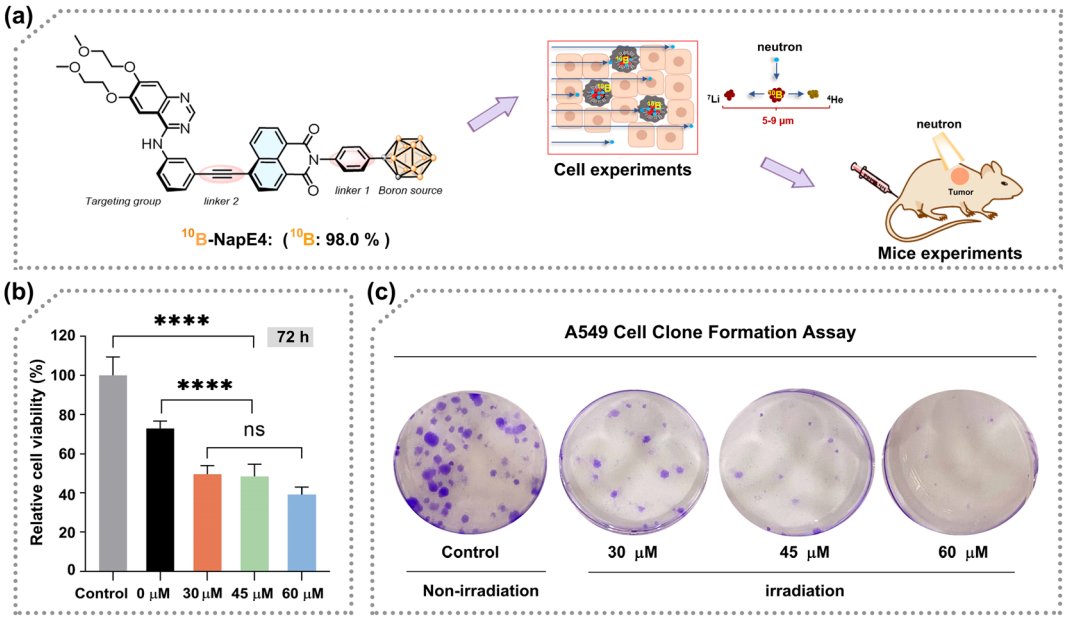

Fig. 5 (a) ^{10}B-NapE4 instead of NapE4 for neutron irradiation experiments. (b) A549 cell viability observed after 72 hours post-26 minute neutron irradiation exposure. *P* values = ****$p < 0.0001$; ***$p < 0.001$; ns: no significance. (c) The clone formation assay of irradiated A549 cells observed at the 14th day. Note: The control group was not exposed to neutron irradiation with no boron delivery agents applied.

26 min exposure) and 46.7% (for 17 min exposure) with a concentration of 60 μM of **^{10}B-NapE4** (Table S10†). Moreover, the colony formation assay also showed excellent dose dependence. After 14 days of culture, the colony formation rate was decreased by 47.0% with a concentration of 60 μM in comparison to the control group with no boron delivery agents and irradiation applied (Fig. 5c, S18c, d and Table S11†). These results indicate that **^{10}B-NapE4** can efficiently inhibit the proliferation and colony formation of tumor cells after neutron irradiation, demonstrating its suitability for further *in vivo* investigations.

Neutron irradiation of tumor-bearing mice

Similarly, the boron content of the selected organs after 24 h injection of **^{10}B-NapE4** (15 mg kg^{-1}) in the tumor-bearing mice ($n = 3$) needs to be tested again to ensure the consistent boron content accumulation *in vivo* after replacement of **NapE4**. The ^{10}B accumulation in tumors was 22.66 ± 3.28 μg g^{-1}, and the T/N and T/B ratios were 35.42 ± 1.84 and 28.93 ± 2.29, respectively, similar to those in **NapE4** (Table S12†). Then **^{10}B-NapE4** was intravenously administered at a dose of 15 mg kg^{-1} body weight in subcutaneous A549 tumor-bearing mice. After 24 h the mice were exposed to different doses of neutron beams (L BNCT; M BNCT; H BNCT; Fig. S19 and Table S13†). For comparison, three other groups were also set up as the control, **^{10}B-NapE4** injection only (or drug only), and neutron irradiation only (2.0 Gy) (or neutron only), respectively. Firstly, the biosafety of the irradiation was assessed by measuring the body weight of the mice. No obvious adverse effects or abnormalities were observed, indicating that **^{10}B-NapE4** is well tolerated (Fig. 6a). Secondly, no evident effect on tumor growth was observed in the three comparison groups. In sharp contrast, in the three **^{10}B-NapE4** + irradiation groups, obvious suppression of tumor growth was observed after 10 days of irradiation (Fig. 6b and c). In particular, in the H BNCT group, the tumor growth was significantly inhibited at such a low dose of boron delivery agent (15 mg kg^{-1}). Thus, the *in vivo* experimental results demonstrate that **^{10}B-NapE4** is an efficient boron delivery agent. This should be attributed to three factors: (1) **^{10}B-NapE4** is a ^{10}B-enriched species; (2) the Eriotinib targeting plays a crucial role in the selective accumulation of **^{10}B-NapE4** in tumor cells; (3) the real-time imaging detection of **^{10}B-NapE4** accumulation in tumor tissue allows for choosing the best irradiation time.

Mechanistic investigations

We further performed histological and immunohistochemical analyses on the irradiated tumor tissues by H&E, Ki67, γ-H2AX, and P53 staining (Fig. 6d and S20†). H&E staining revealed that the cell nuclei were blurred and fragmented in the **^{10}B-NapE4** + irradiation groups. Ki67 staining showed a low percentage of proliferating cells in the **^{10}B-NapE4** + irradiation groups, in particular in the H BNCT group. In sharp contrast, the three comparison groups had intact cell nuclei and high percentages of Ki67-positive cells (Fig. 6d and e). γ-H2AX is a marker of DNA double-strand breakage induced by radiation. P53 protein is usually activated when DNA is damaged, which then triggers cell apoptosis.[24] Here the results showed that γ-H2AX and P53 expression was significantly increased in M BNCT and H BNCT groups compared to the other groups (Fig. 6f and g). These demonstrate that **^{10}B-NapE4** has apparent antitumor activity by inducing DNA double-strand damage upon neutron irradiation.

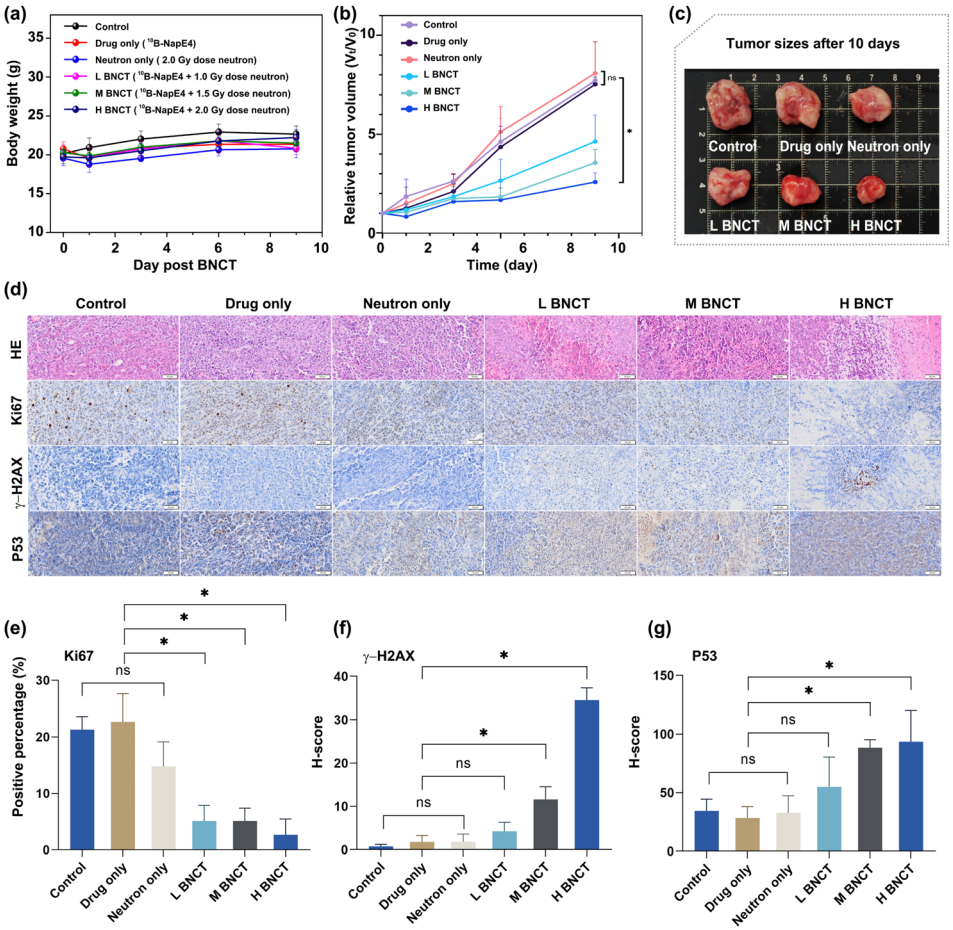

Fig. 6 (a) Weight growth curves of mice after irradiation (0–9 days, L BNCT: ^{10}B-NapE4 + neutron irradiation for 7 minutes = radioactive dose of 1.0 Gy; M BNCT: ^{10}B-NapE4 + neutron irradiation for 10 minutes = radioactive dose of 1.5 Gy; H BNCT: ^{10}B-NapE4 + neutron irradiation for 14 minutes = radioactive dose of 2.0 Gy). (b) Tumor growth curves ($n = 6$) after irradiation (0–9 days). Statistical analysis was conducted by using the one-way ANOVA multiple comparison test with Tukey's method for tumor volumes 9 days post treatment, *$p < 0.05$. (c) Comparison of the explanted tumor size after 10 days of irradiation. (d) Pathological and immunohistochemical results. Representative pathological images of apoptosis and proliferation in tumor tissues. Statistical analysis of (e) Ki67, (f) γ-H2AX, and (g) P53. *P* values = *$p < 0.05$; ns: no significance. Note: the control group was not exposed to neutron irradiation with no boron delivery agents applied.

Conclusions

In this contribution, we demonstrate the successful molecular engineering of a new type of boron delivery agent for BNCT investigations by the "three-in-one" strategy. The three functional groups of carborane, Eriotinib and naphthalimide as the boron source, targeting unit and chromophore exhibit perfect interplay to lead to the expected AIEgens which match the high boron content of a boron delivery agent required by BNCT. AIE imaging has played an important role in finding the optimal neutron irradiation timing for achieving the best treatment and biosafety. This series of boron delivery agents show excellent targeting properties to give rise to a ^{10}B accumulation of over 20 μg g^{-1} and T/N and T/B ratios 20–30 times higher than those (3 : 1) required by BNCT even at a low dose of boron delivery agents of 15 mg kg^{-1}. For comparison, the dose of clinically used BPA for the treatment of melanoma was 600 mg kg^{-1} to give a ^{10}B accumulation of 36 ± 4 μg g^{-1}.[2b] Both *in vitro* and *in vivo* neutron irradiation assessments exhibit highly efficient inhibition on tumor cell growth, and no physical tissue damage and abnormal behavior *in vivo*. The histological and immunohistochemical analyses have verified DNA damage and the following cancer cell apoptosis. The preliminary results have offered an effective strategy for constructing multi-functional boron delivery agents, which may hold significant potential for advanced BNCT platforms.

Data availability

Data supporting this study is available in the ESI† and further details are available from the authors on reasonable request.

Author contributions

Wenli Ma designed and synthesized all the target compounds. Deshuang Tu, Changsheng Lu and Hong Yan supervised the research. Mengmeng Wang performed theoretical calculations. Qinfeng Xu, Yanyang Wang, Yilin Xue, Guoqiang Shao and

Wanhua Guo completed the biological tests. Yuan-Hao Liu and Diyun Shu designed and completed neutron irradiation experiments. All authors discussed the results and revised the manuscript.

Conflicts of interest

There are no conflicts to declare.

Acknowledgements

This work was supported by the National Natural Science Foundation of China (92261202, 91961104 and 21820102004), the Ministry of Science and Technology (2021YFE0114800), the Natural Science Foundation of Jiangsu Province (BZ2022007 and SBZ2022080031), the Nanjing health science and technology development special fund project (YKK21086 and YKK21254), the High-Performance Computational Center of Nanjing University, and Henan Normal University. We are grateful to the Experimental Technologies Center of the Nanjing Institute of Geology and Palaeontology, Chinese Academy of Sciences, for ICP-MS technical assistance. All *in vivo* experiments were approved by the Animal Care and Use Committee and Ethics Committee of Nanjing First Hospital (DWSY-23058362). All animals were acclimatized to the environment for at least one week to reduce stress before all animal experiments.

Notes and references

1 (*a*) C. Lovatt and W. Dugger, *Boron*, Springer, 1984, pp. 389–421, ISBN: 978-1-4684-4777-4; (*b*) S. Hermánek, *Chem. Rev.*, 1992, **92**, 175; (*c*) N. S. Hosmane, *Boron Science: New Technologies and Applications*, CRC, Boca Raton, 2011, ISBN: 978-1-4398-2662-1; (*d*) N. S. Hosmane and R. Eagling, *Handbook of Boron Chemistry in Organometallics, Catalysis, Materials and Medicine*, Imperial College Press/World Scientific Publishing (UK) Ltd., 2018, ISBN: 978-1-78634-441-0.

2 (*a*) N. S. Hosmane, J. A. Maguire, Y. Zhu and M. Takagaki, *Boron and Gadolinium Neutron Capture Therapy for Cancer Treatment*, World Scientific Publishers, Singapore, 2011, Ch. 9, pp. 165–170, ISBN: 978-981-4338-67-7; (*b*) W. Sauerwein, A. Wittig, R. Moss and Y. Nakagawa, *Neutron Capture Therapy*, Springer Heidelberg, New York Dordrecht London, 2012, ISBN: 978-3-642-31333-2; (*c*) M. F. Hawthorne, *Angew. Chem., Int. Ed.*, 1993, **32**, 950–984; (*d*) K. Nedunchezhian, N. Aswath, M. Thiruppathy and S. Thirugnanamurthy, *J. Clin. Diagn. Res.*, 2016, **10**, ZE01–ZE04; (*e*) R. Barth, Z. Zhang and T. Liu, *Cancer Commun.*, 2018, **38**, 36; (*f*) L. E. Farr, W. H. Sweet, J. S. Robertson, C. G. Foster, H. B. Locksley, D. L. Sutherland, M. L. Mendelsohn and E. E. Stickley, *Am. J. Roentgenol.*, 1954, **71**, 279–293; (*g*) H. R. Snyder, A. J. Reedy and W. J. Lennarz, *J. Am. Chem. Soc.*, 1958, **80**, 835–838; (*h*) C. Perks, A. Mill, G. Constantine, K. Harrison and J. Gibson, *Br. J. Radiol.*, 1988, **61**, 1115–1126; (*i*) J. Goodman, J. McGregor, N. Clendenon, R. Gahbauer, R. Barth, A. Soloway and R. Fairchild, *Neurosurgery*, 1990, **27**, 383–388.

3 (*a*) M. Suzuki, *Int. J. Clin. Oncol.*, 2020, **25**, 43–50; (*b*) R. F. Barth and J. C. Grecula, *Appl. Radiat. Isot.*, 2020, **160**, 109029; (*c*) J. Bahng, B.-S. Lee, E.-S. Kim, S. Park and H.-K. Park, *Rev. Sci. Instrum.*, 2020, **91**, 023323.

4 R. N. Grimes, *Carboranes*, Elsevier, Oxford, 3rd edn, 2016, pp. 283–502, ISBN: 978-0-12-801894-1.

5 (*a*) P. Stockmann, M. Gozzi, R. Kuhnert, M. B. Sarosi and E. Hey-Hawkins, *Chem. Soc. Rev.*, 2019, **48**, 3497; (*b*) F. Issa, M. Kassiou and L. M. Rendina, *Chem. Rev.*, 2011, **111**, 5701–5722; (*c*) J. Brynda, P. Mader, V. Šícha, M. Fábry, K. Poncová, M. Bakardiev, B. Grüner, P. Cígler and P. Řezáčová, *Angew. Chem., Int. Ed.*, 2013, **52**, 13760–13763; (*d*) Y. Yin, N. Ochi, T. W. Craven, D. Baker, N. Takigawa and H. Suga, *J. Am. Chem. Soc.*, 2019, **141**, 19193–19197; (*e*) Y. Zhu, A. Peng, K. Carpenter, J. A. Maguire, N. S. Hosmane and M. Takagaki, *J. Am. Chem. Soc.*, 2005, **127**, 9875–9880; (*f*) S. Li, Z. Wang, Y. Wei, C. Wu, S. Gao, H. Jiang, X. Zhao, H. Yan and X. Wang, *Biomaterials*, 2013, **34**, 902–911; (*g*) R. Varkhedkar, F. Yang, R. Dontha, J. Zhang, J. Liu, B. Spingler, S. van der Veen and S. Duttwyler, *ACS Cent. Sci.*, 2022, **8**, 322–331; (*h*) C. Wu, H. Ye, W. Bai, Q. Li, D. Guo, G. Lv, H. Yan and X. M. Wang, *Bioconjugate Chem.*, 2011, **22**, 16–25; (*i*) N. Meher, K. Seo, S. Wang, A. P. Bidkar, M. Fogarty, S. Dhrona, X. Huang, R. Tang, C. Blaha, M. J. Evans, D. R. Raleigh, Y.-W. Jun, H. F. VanBrocklin, T. A. Desai, D. M. Wilson, T. Ozawa and R. R. Flavell, *ACS Appl. Mater. Interfaces*, 2021, **13**, 54739–54752; (*j*) S. Li, C. Wu, X. Zhao, H. Jiang, H. Yan and X. M. Wang, *J. Biomed. Nanotechnol.*, 2013, **9**, 393–402; (*k*) R. Li, J. Zhang, J. Guo, Y. Xu, K. Duan, J. Zheng, H. Wan, Z. Yuan and H. Chen, *Mol. Pharm.*, 2020, **17**, 202–211; (*l*) H. Dou, W. Zhong, Y. Hou and H. Yan, *Bioorg. Med. Chem.*, 2012, **20**, 4693–4700; (*m*) P. Cígler, M. Kožíšek, P. Řezáčová, J. Brynda, Z. Otwinowski, J. Pokorná, J. Plešek, B. Grüner, L. Marešová, M. Máša, J. Sedláček, J. Bodem, H.-G. Kräusslich, V. Král and J. Konvalinka, *Proc. Natl. Acad. Sci. U. S. A.*, 2005, **102**, 15394–15399; (*n*) C. Wu, L. Shi, Q. Li, H. Jiang, M. Selke, H. Yan and X. M. Wang, *Nanomedicine*, 2012, **8**, 860–869; (*o*) S. Wang, C. Blaha, R. Santos, T. Huynh, T. R. Hayes, D. R. Beckford-Vera, J. E. Blecha, A. S. Hong, M. Fogarty, T. A. Hope, D. R. Raleigh, D. M. Wilson, M. J. Evans, H. F. VanBrocklin, T. Ozawa and R. R. Flavell, *Mol. Pharm.*, 2019, **16**, 3831–3841; (*p*) G. Zheng, C. Wu, H. Ye, H. Yan and X. M. Wang, *J. Nanobiotechnol.*, 2011, **9**, 1–8; (*q*) S. Fujii, H. Masuno, Y. Taoda, A. Kano, A. Wongmayura, M. Nakabayashi, N. Ito, M. Shimizu, E. Kawachi, T. Hirano, Y. Endo, A. Tanatani and H. Kagechika, *J. Am. Chem. Soc.*, 2011, **133**, 20933–20941.

6 (*a*) R. Núñez, M. Tarres, A. Ferrer-Ugalde, F. F. de Biani and F. Teixidor, *Chem. Rev.*, 2016, **116**, 14307–14378; (*b*) J. F. Valliant, K. J. Guenther, A. S. King, P. Morel, P. Schaffer, O. O. Sogbein and K. A. Stephenson, *Coord. Chem. Rev.*, 2002, **232**, 173–230; (*c*) A. Marfavi,

P. Kavianpour and L. M. Rendina, *Nat. Rev. Chem.*, 2022, **6**, 486–504; (*d*) A. Saha, E. Oleshkevich, C. Viñas and F. Teixidor, *Adv. Mater.*, 2017, **29**, 1704238; (*e*) J. Ochi, K. Tanaka and Y. Chujo, *Angew. Chem., Int. Ed.*, 2023, **62**, e202214397; (*f*) D. Tu, S. Cai, C. Fernandez, H. Ma, X. Wang, H. Wang, C. Ma, H. Yan, C. Lu and Z. An, *Angew. Chem., Int. Ed.*, 2019, **58**, 9129–9133; (*g*) R. Furue, T. Nishimoto, I. S. Park, J. Lee and T. Yasuda, *Angew. Chem., Int. Ed.*, 2016, **55**, 7171–7175; (*h*) D. Tu, P. Leong, S. Guo, H. Yan, C. Lu and Q. Zhao, *Angew. Chem., Int. Ed.*, 2017, **56**, 11370–11374; (*i*) J. Tong, Y. Cao, Y.-W. Zhang, P. Wang, P. Wang, X.-J. Liao, W. Zhang, Y. Wang, Y.-X. Zheng, J.-J. Zhu and Y. Pan, *Angew. Chem., Int. Ed.*, 2022, **61**, e202209438; (*j*) X. Wei, M. Zhu, Z. Cheng, M. Lee, H. Yan and C. J. Xu, *Angew. Chem., Int. Ed.*, 2019, **58**, 3162–3166; (*k*) J. Ochi, K. Tanaka and Y. Chujo, *Angew. Chem., Int. Ed.*, 2020, **59**, 9841–9855; (*l*) Y. H. Lee, J. Park, J. Lee, S. U. Lee and M. H. Lee, *J. Am. Chem. Soc.*, 2015, **137**, 8018–8021; (*m*) L. Ji, S. Riese, A. Schmiedel, M. Holzapfel, M. Fest, J. Nitsch, B. F. E. Curchod, A. Friedrich, L. Wu, H. H. Al Mamari, S. Hammer, J. Pflaum, M. A. Fox, D. J. Tozer, F. Maik, C. Lambert and T. B. Marder, *Chem. Sci.*, 2022, **13**, 5205–5219; (*n*) S. Sinha, Z. Kelemen, E. Humpfner, I. Ratera, J. P. Malval, J. P. Jurado, C. Viñas, F. Teixidor and R. Núñez, *Chem. Commun.*, 2022, **58**, 4016–4019; (*o*) K.-R. Wee, W.-S. Han, D. Cho, S. Kwon, C. Pac and S. O. Kang, *Angew. Chem., Int. Ed.*, 2012, **124**, 2731–2734; (*p*) J. C. Axtell, K. O. Kirlikovali, P. I. Djurovich, D. Jung, V. T. Nguyen, B. Munekiyo, A. T. Royappa, A. L. Rheingold and A. M. Spokoyny, *J. Am. Chem. Soc.*, 2016, **138**, 15758–15765.

7 (*a*) A. Barba-Bon, G. Salluce, I. Lostalé-Seijo, K. I. Assaf, A. Hennig, J. Montenegro and W. M. Nau, *Nature*, 2022, **603**, 637–642; (*b*) C. Shi, H. Sun, X. Tang, W. Lv, H. Yan, Q. Zhao, J. Wang and W. Huang, *Angew. Chem., Int. Ed.*, 2013, **52**, 13434–13438; (*c*) M. Couto, M. F. Garcia, C. Alamon, M. Cabrera, P. Cabral, A. Merlino, F. Teixidor, H. Cerecetto and C. Viñas, *Chem.–Eur. J.*, 2018, **24**, 3122–3126; (*d*) M. Couto, I. Mastandrea, M. Cabrera, P. Cabral, F. Teixidor, H. Cerecetto and C. Viñas, *Chem.–Eur. J.*, 2017, **23**, 9233–9238; (*e*) M. Scholz, A. L. Blobaum, L. J. Marnett and E. Hey-Hawkins, *Bioorg. Med. Chem.*, 2011, **19**, 3242–3248; (*f*) C. Shi, D. Tu, Q. Yu, H. Liang, Y. Liu, Z. Li, H. Yan, Q. Zhao and W. Huang, *Chem.–Eur. J.*, 2014, **20**, 16550–16557; (*g*) D. J. Worm, S. Els-Heindl, M. Kellert, R. Kuhnert, S. Saretz, J. Koebberling, B. Riedl, E. Hey-Hawkins and A. G. Beck-Sickinger, *J. Pept. Sci.*, 2018, **24**, e3119; (*h*) L. Zhu, X. Tang, Q. Yu, W. Lv, H. Yan, Q. Zhao and W. Huang, *Chem.–Eur. J.*, 2015, **21**, 4721–4730; (*i*) X. Li, X. Tong, Y. Yin, H. Yan, C. Lu, W. Huang and Q. Zhao, *Chem. Sci.*, 2017, **8**, 5930–5940; (*j*) L. Zhu, W. Lv, S. Liu, S. Li, H. Yan, Q. Zhao and W. Huang, *Chem. Commun.*, 2013, **49**, 10638–10640; (*k*) J. Wang, L. Chen, J. Ye, Z. Li, H. Jiang, H. Yan, M. Y. Stogniy, I. B. Sivaev, V. I. Bregadze and X. Wang, *Biomacromolecules*, 2017, **18**, 1466–1472; (*l*) C. Shi, H. Sun, Q. Jiang, Q. Zhao, J. Wang, W. Huang and H. Yan, *Chem. Commun.*, 2013, **49**, 4746–4748.

8 (*a*) M. F. Hawthorne, J. I. Zink, J. M. Skelton, M. J. Bayer, C. Liu, E. Livshits, R. Baer and D. Neuhauser, *Science*, 2004, **303**, 1849–1851; (*b*) A. M. Spokoyny, C. W. Machan, D. J. Clingerman, M. S. Rosen, M. J. Wiester, R. D. Kennedy, C. L. Stern, A. A. Sarjeant and C. A. Mirkin, *Nat. Chem.*, 2011, **3**, 590–596; (*c*) H. S. Ban and H. Nakamura, *Chem. Rev.*, 2015, **15**, 616–635; (*d*) M. Scholz and E. Hey-Hawkins, *Chem. Rev.*, 2011, **111**, 7035–7062; (*e*) Y. Liu, W. Dong, Z. H. Li and H. Wang, *Chem*, 2021, **7**, 1843–1851; (*f*) A. M. Spokoyny, T. C. Li, O. K. Farha, C. W. Machan, C. She, C. L. Stern, T. J. Marks, J. T. Hupp and C. A. Mirkin, *Angew. Chem., Int. Ed.*, 2010, **49**, 5339–5343; (*g*) Z. Wang, X. Gou, Q. Shi, K. Liu, X. Chang, G. Wang, W. Xu, S. Lin, T. Liu and Y. Fang, *Angew. Chem., Int. Ed.*, 2022, **61**, e202207619; (*h*) N. V. Nghia, S. Jana, S. Sujith, J. Y. Ryu, J. Lee, S. U. Lee and M. H. Lee, *Angew. Chem., Int. Ed.*, 2018, **57**, 12483–12488; (*i*) X. Tan, X. Wang, Z. H. Li and H. Wang, *J. Am. Chem. Soc.*, 2022, **144**, 23286–23291; (*j*) K.-R. Wee, Y.-J. Cho, S. Jeong, S. Kwon, J.-D. Lee, I.-H. Suh and S. O. Kang, *J. Am. Chem. Soc.*, 2012, **134**, 17982–17990; (*k*) J. J. Schwartz, A. M. Mendoza, N. Wattanatorn, Y. Zhao, V. T. Nguyen, A. M. Spokoyny, C. A. Mirkin, T. Baše and P. S. Weiss, *J. Am. Chem. Soc.*, 2016, **138**, 5957–5967; (*l*) M. P. Grzelczak, S. P. Danks, R. C. Klipp, D. Belic, A. Zaulet, C. Kunstmann-Olsen, D. F. Bradley, T. Tsukuda, C. Viñas, F. Teixidor, J. J. Abramson and M. Brust, *ACS Nano*, 2017, **11**, 12492–12499; (*m*) W. Li, H. Chen, M. Shen, Z. Yang, Z. Fan, J. Xiao, J. Chen, H. Zhang, Z. Wang and X. Wang, *Small*, 2022, **18**, 2108055; (*n*) Y. Xu, Y. Yang, Y. Liu, Z. H. Li and H. Wang, *Nat. Catal.*, 2023, **6**, 16–22.

9 (*a*) A. G. Beck-Sickinger, D. P. Becker, O. Chepurna, B. Das, S. Flieger, E. Hey-Hawkins, N. S. Hosmane, S. S. Jalisatgi, H. Nakamura, R. Patil, M. d. G. H. Vicente and C. Viñas, *Cancer Biother. Radiopharm.*, 2023, **38**, 160–172; (*b*) K. Hu, Z. Yang, L. Zhang, L. Xie, L. Wang, H. Xu, L. Josephson, S. H. Liang and M.-R. Zhang, *Coord. Chem. Rev.*, 2020, **405**, 213139; (*c*) Y. Shi, Q. Fu, J. Li, H. Liu, Z. Zhang, T. Liu and Z. Liu, *ACS Appl. Mater. Interfaces*, 2020, **12**, 55564–55573; (*d*) Y. Shi, J. Li, Z. Zhang, D. Duan, Z. Zhang, H. Liu, T. Liu and Z. Liu, *ACS Appl. Mater. Interfaces*, 2018, **10**, 43387–43395; (*e*) J. Chen, Q. Dai, Q. Yang, X. Bao, Y. Zhou, H. Zhong, L. Wu, T. Wang, Z. Zhang, Y. Lu, Z. Zhang, M. Lin, M. Han and Q. Wei, *J. Nanobiotechnol.*, 2022, **20**, 102.

10 (*a*) Y. Wang, J. Nie, W. Fang, L. Yang, Q. Hu, Z. Wang, J. Z. Sun and B. Z. Tang, *Chem. Rev.*, 2020, **120**, 4534–4577; (*b*) J. Mei, N. L. C. Leung, R. T. K. Kwok, J. W. Y. Lam and B. Z. Tang, *Chem. Rev.*, 2015, **115**, 11718–11940; (*c*) Z. Zhao, H. Zhang, J. Lam and B. Z. Tang, *Angew. Chem., Int. Ed.*, 2020, **59**, 9888–9907; (*d*) X. Cai and B. Liu, *Angew. Chem., Int. Ed.*, 2020, **59**, 9868–9886; (*e*) B. Liu and B. Z. Tang, *Angew. Chem., Int. Ed.*, 2020, **59**, 9788–9789; (*f*) S. Xu, Y. Duan and B. Liu, *Adv. Mater.*, 2020, **32**, 1903530; (*g*) B. Li, C. Liu, W. Pan, J. She, J. Guo, T. Lun, J. Feng, B. Situ, T. An, Y. Zhang and L. Zheng, *Biosens. Bioelectron.*, 2020, **168**, 112520.

11 (*a*) K. Wang, H. Gao, Y. Zhang, H. Yan, J. Si, X. Mi, S. Xia, X. Feng, D. Liu, D. Kong, T. Wang and D. Ding, *Adv. Mater.*, 2021, **34**, 2106994; (*b*) J. Qi, C. Chen, D. Ding and B. Z. Tang, *Adv. Healthcare Mater.*, 2018, **7**, 1800477; (*c*) Y. Wu, J. Li, Z. Shen, D. Wang, R. Dong, J. Zhang, Y. Pan, Y. Li, D. Wang and B. Z. Tang, *Angew. Chem., Int. Ed.*, 2022, **61**, e202212386; (*d*) J. Dai, X. Dong, Q. Wang, X. Lou, F. Xia and S. Wang, *Adv. Healthcare Mater.*, 2021, **10**, 2101036; (*e*) Y. Li, R. Tang, X. Liu, J. Gong, Z. Zhao, Z. Sheng, J. Zhang, X. Li, G. Niu, R. T. K. Kwok, W. Zheng, X. Jiang and B. Z. Tang, *ACS Nano*, 2020, **14**, 16840–16853; (*f*) Y. Cheng, A. Clark, J. Zhou, T. He, Y. Li, R. Borum, M. Creyer, M. Xu, Z. Jin, J. Zhou, W. Yim, Z. Wu, P. Fajtová, A. J. O'Donoghue, A. Carlin and J. Jokerst, *ACS Nano*, 2022, **16**, 12305–12317.

12 (*a*) Y. Dong, B. Liu and Y. Yuan, *J. Controlled Release*, 2018, **290**, 129–137; (*b*) D. Zhang, Y. Fan, H. Chen, S. Trépout and M.-H. Li, *Angew. Chem., Int. Ed.*, 2019, **58**, 10260–10265; (*c*) H. Jin, H. Li, Z. Zhu, J. Huang, Y. Xiao and Y. Yan, *Angew*, 2020, **59**, 10081–11008; (*d*) M.-M. Zhang, X.-Y. Dong, Z.-Y. Wang, H.-Y. Li, S.-J. Li, X. Zhao and S.-Q. Zang, *Angew. Chem., Int. Ed.*, 2020, **59**, 10052–10058; (*e*) P. Sun, B. Han, H. Li, C. Zhang, X. Xin, J. Dou, Z. Gao and D. Sun, *Angew. Chem., Int. Ed.*, 2022, **61**, e20220018; (*f*) Y. Jin, Q. Peng, J. Xie, K. Li and S.-Q. Zang, *Angew. Chem., Int. Ed.*, 2023, **62**, e202301; (*g*) Y. Wang, Y. Zhang, J. Wang and X. Liang, *Adv. Drug Delivery Rev.*, 2019, **143**, 161–176.

13 (*a*) C. Chen, X. Ni, H. Tian, Q. Liu, D. Guo and D. Ding, *Angew. Chem., Int. Ed.*, 2020, **59**, 10008–10012; (*b*) H. Li, Q. Yao, F. Xu, Y. Li, D. Kim, J. Chung, G. Baek, X. Wu, P. F. Hillman, E. Y. Lee, H. Ge, J. Fan, J. Wang, S. Nam, X. Peng and J. Yoon, *Angew. Chem., Int. Ed.*, 2020, **59**, 10186–10195; (*c*) L. Liu, C. Li, J. Gong, Y. Zhang, W. Ji, L. Feng, G. Jiang, J. Wang and B. Z. Tang, *Angew. Chem., Int. Ed.*, 2023, e202307776; (*d*) X. Ni, X. Zhang, X. Duan, H. Zheng, X. Xue and D. Ding, *Nano Lett.*, 2019, **19**, 318–330; (*e*) W. Wu, Y.-Q. Yang, Y. Yang, Y.-M. Yang, H. Wang, K. Zhang, L. Guo, H. Ge, J. Liu and H. Feng, *Int. J. Nanomed.*, 2019, **14**, 3571–3582.

14 (*a*) M. Zhang, W. Wang, M. Mohammadniaei, T. Zheng, Q. Zhang, J. Ashley, S. Liu, Y. Sun and B. Z. Tang, *Adv. Mater.*, 2021, **3**, 2008802; (*b*) K.-N. Wang, L.-Y. Liu, D. Mao, M.-X. Hou, C.-P. Tan, Z.-W. Mao and B. Liu, *Angew. Chem., Int. Ed.*, 2022, **61**, e20211460; (*c*) M. Wu, X. Liu, H. Chen, Y. Duan, J. Liu, Y. Pan and B. Liu, *Angew. Chem., Int. Ed.*, 2021, **60**, 9093–9098; (*d*) D. Zhu, Y. Duo, M. Suo, Y. Zhao, L. Xia, Z. Zheng, Y. Li and B. Z. Tang, *Angew. Chem., Int. Ed.*, 2020, **59**, 13836–13843; (*e*) M. Lee, E. Yu, D. Yan, J. Chau, Q. Wu, J. Lam, D. Ding, R. Kwok, D. Wang and B. Z. Tang, *ACS Nano*, 2023, **17**, 17004–17020, DOI: **10.1021/acsnano.3c04266**; (*f*) R. Xu, W. Chi, Y. Zhao, Y. Tang, X. Jing, Z. Wang, Y. Zhou, Q. Shen, J. Zhang, Z. Yang, D. Dang and L. Meng, *ACS Nano*, 2022, **16**, 20151–20162; (*g*) X. He, B. Situ, M. Gao, S. Guan, B. He, X. Ge, S. Li, M. Tao, H. Zou, B. Z. Tang and L. Zheng, *Small*, 2019, **15**, 1905080; (*h*) Y. Yang, L. Wang, H. Cao, Q. Li, Y. Li, M. Han, H. Wang and J. Li, *Nano Lett.*, 2019, **19**, 1821–1826.

15 (*a*) C. Chen, X. Ni, S. Jia, Y. Liang, X. Wu, D. Kong and D. Ding, *Adv. Mater.*, 2019, **31**, 1904914; (*b*) D. Yan, M. Wang, Q. Wu, N. Niu, M. Li, R. Song, J. Rao, M. Kang, Z. Zhang, F. Zhou, D. Wang and B. Z. Tang, *Angew. Chem., Int. Ed.*, 2022, **61**, e202202614; (*c*) G. Ma, Z. Liu, C. Zhu, H. Chen, R. Kwok, P. Zhang, B. Z. Tang, L. Cai and P. Gong, *Angew. Chem., Int. Ed.*, 2022, **61**, e202207; (*d*) D. Mao, F. Hu, Z. Yi, Kenry, S. Xu, S. Yan, Z. Luo, W. Wu, Z. Wang, D. Kong, X. Liu and B. Liu, *Sci. Adv.*, 2020, **26**, eabb2712; (*e*) S. Wang, W. Wu, P. Manghnani, S. Xu, Y. Wang, C. Goh, L. G. Ng and B. Liu, *ACS Nano*, 2019, **13**, 3095–3105.

16 (*a*) Y. Hong, W. Geng, T. Zhang, G. Gong, C. Li, C. Zheng, F. Liu, J. Qian, M. Chen and B. Z. Tang, *Angew. Chem., Int. Ed.*, 2022, **61**, e202209590; (*b*) S. Song, Y. Wang, Y. Zhao, W. Huang, F. Zhang, S. Zhu, Q. Wu, S. Fu, B. Z. Tang and D. Wang, *Matter*, 2022, **5**, 2847–2863; (*c*) X. Fan, Q. Xia, S. Liu, Z. Zheng, Y. Zhang, T. Wu, Y. Li, G. Tang, B. Z. Tang, J. Qian and H. Lin, *Mater. Today Bio*, 2022, **16**, 100399.

17 (*a*) Z. Sun, J. Liu, Y. Li, X. Lin, Y. Chu, W. Wang, S. Huang, W. Li, J. Peng, C. Liu, L. Cai, W. Deng, C. Sun and G. Deng, *Adv. Mater.*, 2023, **35**, 2208555; (*b*) G. Wang, L. Zhou, P. Zhang, E. Zhao, L. Zhou, D. Chen, J. Sun, X. Gu, W. Yang and B. Z. Tang, *Angew. Chem., Int. Ed.*, 2020, **59**, 10122–10128; (*c*) Z. Wang, L. Yu, Y. Wang, C. Wang, Q. Mu, X. Liu, M. Yu, K.-N. Wang, G. Yao and Z. Yu, *Adv. Sci.*, 2022, **9**, 2104793; (*d*) H. Cao, H. Gao, L. Wang, Y. Cheng, X. Wu, X. Shen, H. Wang, Z. Wang, P. Zhan, J. Liu, Z. Li, D. Kong, Y. Shi, D. Ding and Y. Wang, *ACS Nano*, 2022, **16**, 13992–14006; (*e*) J. Dai, M. Wu, Q. Wang, S. Ding, X. Dong, L. Xue, Q. Zhu, J. Zhou, F. Xia, S. Wang and Y. Hong, *Natl. Sci. Rev.*, 2021, **8**, nwab039.

18 (*a*) N. Kuthala, R. Vankayala, Y.-N. Li, C.-S. Chiang and K. C. Hwang, *Adv. Mater.*, 2017, **29**, 1700850; (*b*) L. Li, J. Li, Y. Shi, P. Du, Z. Zhang, T. Liu, R. Zhang and Z. Liu, *ACS Nano*, 2019, **13**, 13843–13852; (*c*) J. Li, Q. Sun, C. Lu, H. Xiao, Z. Guo, D. Duan, Z. Zhang, T. Liu and Z. Liu, *Nat. Commun.*, 2022, **13**, 2143; (*d*) J. Li, J. Kong, S. Ma, J. Li, M. Mao, K. Chen, Z. Chen, J. Zhang, Y. Chang, H. Yuan, T. Liu, Z. Zhang and G. Xing, *Adv. Funct. Mater.*, 2021, **31**, 2100969; (*e*) Z. Wang, Z. Chen, Z. Zhang, J. Li, K. Chen, H. Liang, L. Lv, Y. Chang, S. Liu, W. Yang, Z. Yang, H. Yuan, X. Meng, T. Liu, F. Wang, J. Li and G. Xing, *Nano Today*, 2022, **45**, 101558; (*f*) Y. Wang, G. Reina, H. G. Kang, X. Chen, Y. Zou, Y. Ishikawa, M. Suzuki and N. Komatsu, *Small*, 2022, **18**, 2204044; (*g*) L. Dai, J. Liu, X. Zhao, Y. Li, S. Zhou, L. Yuan, D. Shu, L. Pan, Y.-H. Liu and Z. Qian, *Adv. Funct. Mater.*, 2023, 2214145; (*h*) S. Scaramuzza, C. Faria, V. Coviello, D. Forrer, L. Artiglia, D. Badocco, P. Pastore, P. Ghigna, I. Postuma, L. Cansolino, C. Ferrari, S. Bortolussi, R. Vago, A. E. Spinelli, M. Bekić, M. Čolić and V. Amendola, *Adv. Funct. Mater.*, 2023, 2303366; (*i*) Y. Zhang, H. Kang, H. Xu, H. Luo, M. Suzuki, Q. Lan, X. Chen, N. Komatsu and L. Zhao, *Adv. Funct. Mater.*, 2023, 2301479; (*j*) T. Nomoto, Y. Inoue, Y. Yao, M. Suzuki,

K. Kanamori, H. Takemoto, M. Matsui, K. Tomoda and N. Nishiyama, *Sci. Adv.*, 2020, **6**, eaaz1722; (*k*) A. Kim, M. Suzuki, Y. Matsumoto, N. Fukumitsu and Y. Nagasaki, *Biomaterials*, 2021, **268**, 120551; (*l*) Q. Dai, Q. Yang, X. Bao, J. Chen, M. Han and Q. Wei, *Mol. Pharmaceutics*, 2022, **19**, 363–377; (*m*) P. Coghi, J. Li, N. S. Hosmane and Y. Zhu, *Med. Res. Rev.*, 2023, 1–22; (*n*) Y. Shi, Z. Guo, Q. Fu, X. Shen, Z. Zhang, W. Sun, J. Wang, J. Sun, Z. Zhang, T. Liu, Z. Gu and Z. Liu, *Nat. Commun.*, 2023, **14**, 4; (*o*) K. Chen, S. Liu, L. Lv, J. Tong, J. Chen, H. Liang, Y. Wang, F. Hu, Q. Liu, H. Li, Z. Chen, J. Li, Z. Wang, Y. Chang, J. Li, H. Yuan, S. Fu, T. Liang and G. Xing, *Nano Today*, 2023, **52**, 101995; (*p*) Z. Wang, R. Lei, Z. Zhang, Z. Chen, J. Zhang, M. Mao, J. Li, H. Tang, M. Li, X. Luo, J. Yang, R. Yan, Q. Liu, L. Lv, K. Chen, Y. Chang, H. Yuan, T. Liu, J. Tong, L. Zhu, T. Liang, W. Zhang, J. Li and G. Xing, *ACS Appl. Mater. Interfaces*, 2024, **16**, 3232–3242.

19 (*a*) S. M. Thomasa and J. R. Grandis, *Cancer Treat. Rev.*, 2004, **30**, 255–268; (*b*) O. Chahrour, D. Cairns and Z. Omran, *Mini-Rev. Med. Chem.*, 2012, **12**, 399–411.

20 (*a*) M. Couto, C. Alamón, S. Nievas, M. Perona, M. A. Dagrosa, F. Teixidor, P. Cabral, C. Viñas and H. Cerecetto, *Chem.–Eur. J.*, 2020, **26**, 14335–14340; (*b*) R. R. Cheruku, J. Cacaccio, F. A. Durrani, W. A. Tabaczynski, R. Watson, K. Siters, J. R. Missert, E. C. Tracy, M. Dukh, K. Guru, R. C. Koya, P. Kalinski, H. Baumann and R. K. Pandey, *J. Med. Chem.*, 2021, **64**, 741–767; (*c*) C. Alamón, B. Dávila, M. F. García, S. Nievas, M. A. Dagrosa, S. Thorp, M. Kovacs, E. Trias, R. Faccio, M. Gabay, N. Zeineh, A. Weizman, F. Teixidor, C. Viñas, M. Gavish, H. Cerecetto and M. Couto, *Mol. Pharmaceutics*, 2023, **20**, 2702–2713; (*d*) C. Yewale, D. Baradia, I. Vhora, S. Patil and A. Misra, *Biomaterials*, 2013, **34**, 8690–8707; (*e*) P. Sidaway, *Nat. Rev. Clin. Oncol.*, 2018, **15**, 654; (*f*) B. Mandal, P. Balabathula, N. Mittal, G. C. Wood and H. Bhattacharjee, *J. Fluoresc.*, 2012, **22**, 1425–1429.

21 (*a*) S. Banerjee, E. B. Veale, C. M. Phelan, S. A. Murphy, G. M. Tocci, L. J. Gillespie, D. O. Frimannsson, J. M. Kelly and T. Gunnlaugsson, *Chem. Soc. Rev.*, 2013, **42**, 1601–1618; (*b*) Z. Zhu, D. Tian, P. Gao, K. Wang, Y. Li, X. Shu, J. Zhu and Q. Zhao, *J. Am. Chem. Soc.*, 2018, **140**, 17484–17491; (*c*) B. Lozano-Torres, I. Galiana, M. Rovira, E. Garrido, S. Chaib, A. Bernardos, D. Muñoz-Espín, M. Serrano, R. Martínez-Máñez and F. Sancenón, *J. Am. Chem. Soc.*, 2017, **139**, 8808–8811; (*d*) N. I. Georgiev and V. B. Bojinov, *J. Lumin.*, 2012, **132**, 2235–2241.

22 (*a*) N. Nakashima, M. Murakawa and N. Mataga, *Bull. Chem. Soc. Jpn.*, 1976, **49**, 854–858; (*b*) D. Tu, P. Leong, Z. Li, R. Hu, C. Shi, K. Y. Zhang, H. Yan and Q. Zhao, *Chem. Commun.*, 2016, **52**, 12494–12497.

23 (*a*) T. Lu and F. Chen, *J. Comput. Chem.*, 2012, **33**, 580–592; (*b*) T. Lu and F. Chen, *J. Phys. Chem. A*, 2013, **117**, 3100–3108.

24 (*a*) L. A.-O. Widjaja, R. A. Werner, E. Krischke, H. Christiansen, F. M. Bengel, N. Bogdanova and T. Derlin, *Eur. J. Nucl. Med. Mol. Imaging*, 2023, **50**, 602–612; (*b*) P. L. Vaddavalli and B. Schumacher, *Trends Genet.*, 2022, **38**, 598–612.